Nonintegrable Hamiltonian and Chaotic Electron Motion in Dual-Wiggler Free-Electron Laser with Axial Guiding Field

M. Abu Safa*

Department of Applied Physics, Palestine Polytechnic University, Hebron, P.O. Box 198, Palestine

       *e-mail: mustafa@ppu.edu

A free-electron laser is a laser that has the same optical properties as a conventional laser, such as emitting beams of coherent electromagnetic radiation, which can reach high powers, but uses some very different principles of operation to form the beams. The chaotic motion of electrons causes a considerable decrease in the gain and efficiency of free-electron lasers. In this paper, the Hamiltonian of the dual-wiggler free-electron laser with and without axial guide magnetic field is constructed. Hamilton's equations of motion were derived exactly for both cases. The steady-state solution is also derived and investigated so that the initial conditions of the system are clear. The Poincaré surface-of-section maps were plotted after solving Hamilton's equations of motion numerically, where the chaotic behavior of the system was obvious when the axial field was included while the motion became regular and the Hamiltonian is integrable in the absence of the axial guide magnetic field. Regular orbits are observed clearly for large values of the axial field.

topics: free-electron laser, wigglers, undulators, chaos

1. Introduction

A free-electron laser, or FEL, is a laser that has the same optical properties as a conventional laser, such as emitting beams of coherent electromagnetic radiation, which can reach high powers, but uses some very different principles of operation to form the beams [1]. FEL uses a relativistic electron beam as a lasing medium, which moves freely in a transverse periodic magnetic field called a wiggler (or undulator) [2]. Free-electron lasers have the widest frequency range of any laser type and can be tuned to a large extent. In recent years, a great deal of research, both experimental and theoretical, has been carried out on free-electron lasers (FELs). Experimental and theoretical work has yielded many successful results in laboratories and research centers around the world. FEL is characterized by its special performance, first of all, wide frequency tunability, high frequency, high power, and wide bandwidth [3]. These features are attractive for a variety of medical, industrial, and military applications. FEL radiation is typically caused by electrons passing through a magnetic device called an "undulator" or "wiggler," in which the electrons are forced to perform periodic oscillating trajectories in space [4]. The precise form of the wiggler field can take various configurations, and FELs are constructed with helically polarized and linearly polarized wiggler fields. In this paper, we used a configuration of the so-called dual wiggler, which has two wavelengths and two field strengths [5].

The invention of optical lasers led to a revolution in the field of optics and to the creation of such fields of research as quantum optics. The reason was their unique statistical and coherence properties. The emerging short-wavelength free-electron lasers (FELs) are sources of very bright coherent extreme ultraviolet and X-ray radiation with pulse durations on the order of femtoseconds and are presently considered to be laser sources at these energies. FELs are highly spatially coherent to the first order but, in spite of their name, behave statistically as chaotic sources [6].

The extension of the wavelength range of free-electron laser is an important topic in current FEL research. Using higher harmonics is one way to obtain short wavelengths. Both theory and experiments have proved the feasibility [7–10]. But all of this work was done with planar undulator free-electron lasers. Theoretically, it has been shown that the dual-undulator FEL has the advantage over the planar-polarized undulator FEL in terms of obtaining higher harmonics. The dual undulator is a new type of magnetic structure, which has already been proposed by Varfolomeev and Pitatelev [11].
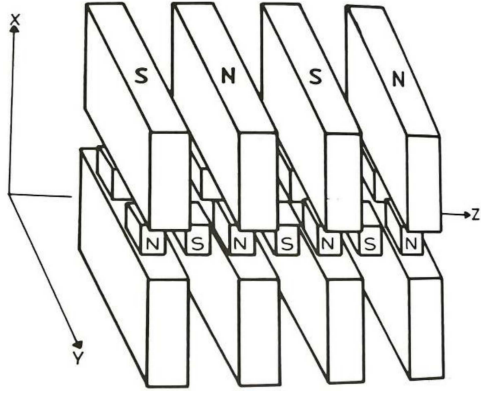
Fig. 1. Schematic diagram of dual wiggler.

Irregular phase-space trajectories of electrons impair the quality of electron beam delivery, reducing the performance of free-electron lasers (FELs). Previous literature has shown that irregularities in the phase-space trajectory of electrons can be induced in several ways, such as changing the wiggler amplitude and inducing sidebands [12]. Based on a Hamiltonian model with a set of self-consistent differential equations, it was shown that the electron beam normalized plasma frequency function not only couples the electron motion to the FEL wave, leading to the evolution of the FEL wavefield, but also that even if the initial energy of the electron is equal to the synchronous energy of the FEL waves, when the normalized plasma frequency has a sufficiently large value, power saturation may occur at large beam currents, and it will also cause irregular waves of electron phase-space trajectories that do not reach power saturation [13].

Hamiltonian chaos has been an active area of research in physics and applied sciences. The classic work of Kolmogorov, Arnold, and Moser (KAM) shows that the generic phase space of nonintegrable classical Hamiltonian systems, subject to small perturbations, contains three types of orbits: stable periodic orbits, stable quasi-periodic orbits (KAM tori), and chaotic orbits [14]. The stability of an electron beam is important to improve the radiation power, gain, and efficiency, and it becomes low-grade due to the high wiggler magnetic field and self-generated fields in a high-power free-electron laser [15]. It is understood that chaotic behavior results from strong dependence on initial conditions [16]. If any error develops in time, the nearby trajectories diverge exponentially, and the orbit depends sensitively on the initial state. A very small randomness in the initial state is sufficient for this to occur. Hamiltonian with N degrees of freedom is integrable if it has N independent constants of motion in involution, e.g., the Poisson bracket of any two constants of them is zero. If the number of constants is less than N, the motion is nonintegrable, and part of the phase space is chaotic [17–19]. FELs are highly spatially coherent to the first-order but,

in spite of their name, behave statistically as chaotic sources. The chaotic motion of electrons causes a considerable decrease in the gain and efficiency of free-electron lasers [20]. The chaotic nature of X-ray free-electron-laser pulses is a major bottleneck that has limited the joint temporal and spectral resolution of spectroscopic measurements [21]. In this paper, we constructed the Hamiltonian of the dual-wiggler free-electron laser with and without the axial guide magnetic field, and Hamilton's equations of motion were derived exactly for both cases. The steady-state solution is also derived and investigated so that the initial conditions of the system are clear. The Poincaré surface-of-section maps were plotted after solving Hamilton's equations of motion, where the chaotic behavior of the system was obvious when the axial field was included while the motion became regular and the Hamiltonian is integrable in the absence of the axial guide magnetic field.

2. Theoretical formulation of the problem

2.1. Dual-wiggler field

In our model, blocks of permanent magnets are joined, as shown in Fig. 1. A guiding axial constant magnetic field is induced into the system to provide more confinement to the beam. The relativistic electron beam propagates near the axis along the z-direction. The magnetic field produced by this configuration, the so-called wiggler, near the axis and the guiding field are [11]

$$\boldsymbol{B} = \boldsymbol{B}_w + \boldsymbol{B}_g$$

$$\boldsymbol{B} = B_{0x} \sin(k_x z)\hat{x} + B_{0y} \sin(k_y z)\hat{y} + B_{0g}\hat{z}, \tag{1}$$

where B_{0x} and B_{0y} are the wiggler magnetic strength in the x- and y-directions, respectively; B_{0g} is the axial guiding field strength; and $k_{x,y} = 2\pi/\lambda_{x,y}$ where $\lambda_{x,y}$ are the wiggler periods in the x- and y-directions. The corresponding vector fields are

$$\boldsymbol{A} = \boldsymbol{A}_w + \boldsymbol{A}_g,$$

$$\boldsymbol{A} = -\frac{B_{0y}}{k_y} \cos(k_y z)\hat{x} + \frac{B_{0x}}{k_x} \cos(k_x z)\hat{y} + B_{0g}x\hat{y}. \tag{2}$$

2.2. The Hamiltonian representation

Frequently, equations of motion of a particle can be written quite simply in Hamiltonian form, in which the system of three second-order equations for the coordinates q_i is represented by a system of six first-order equations for the three-coordinate q_i and the three momenta p_i [19]

$$\frac{\mathrm{d}p_i}{\mathrm{d}t} = -\frac{\partial H}{\partial q_i}, \tag{3}$$

$$\frac{\mathrm{d}q_i}{\mathrm{d}t} = \frac{\partial H}{\partial p_i}, \tag{4}$$

which are called Hamilton's equation of motion. The relativistic Hamiltonian is given by [16]

$$H = \sqrt{m^2c^4 + \left(c\boldsymbol{P} + e\boldsymbol{A}\right)^2} = \gamma mc^2, \tag{5}$$

where γ is the relativistic mass factor. The full form of (5) is given accordingly as

$$H = \left[m^2c^4 + \left(cp_x - \frac{eB_{0y}}{k_y}\cos\left(k_y z\right)\right)^2 \right.$$
$$\left. + \left(cp_y + \frac{eB_{0x}}{k_x}\cos\left(k_x z\right) + eB_{0g}x\right)^2 + (cp_z)^2\right]^{\frac{1}{2}} =$$
$$\gamma mc^2. \tag{6}$$

The Hamiltonian is y-independent, which means that $p_y = \mathrm{const}$, which can be chosen to be zero (i.e., $p_y = 0$).

Another constant of motion is the Hamiltonian since it is time-independent, which means that $H = \mathrm{const} = \gamma mc^2$. Since no new canonical transformation is possible, the third constant of motion is not available and the Hamiltonian is nonintegrable, hence, chaotic orbits are possible.

Normalizing by dividing both sides on mc^2 yields

$$\hat{H} = \left[1 + \left(\frac{p_x}{mc} - \frac{eB_{0y}}{k_y mc^2}\cos(k_y z)\right)^2 \right.$$
$$\left. + \left(\frac{eB_{0x}}{k_x mc^2}\cos(k_x z) + \frac{eB_{0g}}{mc^2}x\right)^2 + \left(\frac{p_z}{mc}\right)^2\right]^{\frac{1}{2}} =$$
$$\left[1 + \left(\hat{p}_x - \hat{A}_{wy}\cos\left(k_y z\right)\right)^2 \right.$$
$$\left. + \left(\hat{A}_{wx}\cos(k_x z) + \Omega x\right)^2 + \hat{p}_z^2\right]^{\frac{1}{2}} = \gamma. \tag{7}$$

Here, $\hat{H} = \frac{H}{mc^2}$, $\hat{p}_x = \frac{p_x}{mc}$, $\hat{p}_y = \frac{p_y}{mc}$, $\hat{p}_z = \frac{p_z}{mc}$, $\hat{A}_{wx} = \frac{eB_{0x}}{k_x mc^2}$, $\hat{A}_{wy} = \frac{eB_{0y}}{k_y mc^2}$, and $\Omega = \frac{eB_{0g}}{mc^2}$.

2.3. Hamilton's equations of motion

The equations of motion of a particle can be written from the Hamiltonian in their x, z, $\hat{p}_x$, and $\hat{p}_z$ forms as follows

$$\frac{\mathrm{d}p_i}{\mathrm{d}t} = -\frac{\partial H}{\partial q_i} \Longrightarrow \frac{d\hat{p}_x}{dt} = -\frac{\partial \hat{H}}{\partial x} \text{ and } \frac{d\hat{p}_z}{dt} = -\frac{\partial \hat{H}}{\partial z},$$

$$\frac{\mathrm{d}q_i}{\mathrm{d}t} = \frac{\partial H}{\partial p_i} \Longrightarrow \frac{\mathrm{d}x}{\mathrm{d}t} = \frac{\partial \hat{H}}{\partial \hat{p}_x} \text{ and } \frac{\mathrm{d}z}{\mathrm{d}t} = \frac{\partial \hat{H}}{\partial \hat{p}_z}, \tag{8}$$

$$\frac{\mathrm{d}\hat{p}_x}{\mathrm{d}t} = -\frac{\partial \hat{H}}{\partial x} = \frac{-\Omega(\hat{A}_{wx}\cos(k_x z) + \Omega x)}{\gamma}, \tag{9}$$

$$\frac{\mathrm{d}\hat{p}_z}{\mathrm{d}t} = -\frac{\partial \hat{H}}{\partial z} = \frac{-k_y\hat{A}_{wy}\sin\left(k_y z\right)(\hat{p}_x - \hat{A}_{wy}\cos\left(k_y z\right))}{\gamma}$$
$$+ \frac{k_x\hat{A}_{wx}\sin\left(k_x z\right)(\hat{A}_{wx}\cos\left(k_x z\right) + \Omega x)}{\gamma}, \tag{10}$$

$$\frac{\mathrm{d}x}{\mathrm{d}t} = \frac{\partial \hat{H}}{\partial \hat{p}_x} = \frac{(\hat{p}_x - \hat{A}_{wy}\cos\left(k_y z\right))}{\gamma}, \tag{11}$$

$$\frac{\mathrm{d}z}{\mathrm{d}t} = \frac{\partial \hat{H}}{\partial \hat{p}_z} = \frac{\hat{p}_z}{\gamma}. \tag{12}$$

The fixed points, or the steady-state orbits, denoted by x_0, z_0, $\hat{p}_{x0}$, $\hat{p}_{z0}$, satisfy the steady-state equations of motion

$$\frac{\mathrm{d}\hat{p}_x}{\mathrm{d}t} = \frac{-\Omega(\hat{A}_{wx}\cos\left(k_x z_0\right) + \Omega x_0)}{\gamma} = 0$$
$$\Longrightarrow -\Omega(\hat{A}_{wx}\cos\left(k_x z_0\right) + \Omega x_0) = 0$$
$$\Longrightarrow x_0 = \frac{-\hat{A}_{wx}\cos\left(k_x z_0\right)}{\Omega}, \tag{13}$$

$$\frac{\mathrm{d}\hat{p}_z}{\mathrm{d}t} = \frac{-k_y\hat{A}_{wy}\sin\left(k_y z_0\right)(\hat{p}_{x0} - \hat{A}_{wy}\cos\left(k_y z_0\right))}{\gamma}$$
$$+ \frac{k_x\hat{A}_{wx}\sin\left(k_x z_0\right)(\hat{A}_{wx}\cos\left(k_x z_0\right) + \Omega x_0)}{\gamma}$$
$$\Longrightarrow -k_y\hat{A}_{wy}\sin\left(k_y z_0\right)(\hat{p}_{x0} - \hat{A}_{wy}\cos\left(k_y z_0\right))$$
$$+ k_x\hat{A}_{wx}\sin\left(k_x z_0\right)(\hat{A}_{wx}\cos\left(k_x z_0\right) + \Omega x_0) = 0, \tag{14}$$

$$\frac{\mathrm{d}x}{\mathrm{d}t} = \frac{(\hat{p}_{x0} - \hat{A}_{wy}\cos\left(k_y z_0\right))}{\gamma} = 0$$
$$\Longrightarrow (\hat{p}_{x0} - \hat{A}_{wy}\cos\left(k_y z_0\right)) = 0$$
$$\Longrightarrow \hat{p}_{x0} = \hat{A}_{wy}\cos\left(k_y z_0\right), \tag{15}$$

$$\frac{\mathrm{d}z}{\mathrm{d}t} = \frac{\hat{p}_{z0}}{\gamma} \Longrightarrow \hat{p}_{z0} = 0. \tag{16}$$

2.4. The Hamiltonian equations of motion without axial guide magnetic field ($\boldsymbol{B}_g = 0$)

The Hamiltonian can be written quite simply in the following form

$$\hat{H} = \left[1 + \left(\hat{p}_x - \hat{A}_{wy}\cos(k_y z)\right)^2 \right.$$
$$\left. + \left(\hat{p}_y + \hat{A}_{wx}\cos(k_x z)\right)^2 + \hat{p}_z^2\right]^{\frac{1}{2}} = \gamma. \tag{17}$$

It is clear that the Hamiltonian is time-independent, so it is a constant of motion

$$\hat{H} = \mathrm{const} = C_1 = \gamma_0. \tag{18}$$

And $\hat{H}$ is x-independent, so $\hat{p}_x$ is constant,

$$\frac{\mathrm{d}\hat{p}_x}{\mathrm{d}t} = -\frac{\partial \hat{H}}{\partial x} = 0 \Longrightarrow \hat{p}_x = \mathrm{const} = C_2. \tag{19}$$

And $\hat{H}$ is y-independent, so $\hat{p}_y$ is constant,

$$\frac{\mathrm{d}\hat{p}_y}{\mathrm{d}t} = -\frac{\partial \hat{H}}{\partial y} = 0 \Longrightarrow \hat{p}_y = \text{const} = C_3. \quad (20)$$

The Hamiltonian is integrable as we already have three constants of motion.

New Hamilton's equations of motion are

$$\frac{\mathrm{d}x}{\mathrm{d}t} = \frac{\partial \hat{H}}{\partial \hat{p}_x} = \frac{(\hat{p}_x - \hat{A}_{wy}\cos{(k_y z)})}{\gamma_0}, \quad (21)$$

$$\frac{\mathrm{d}z}{\mathrm{d}t} = \frac{\partial \hat{H}}{\partial \hat{p}_z} = \frac{\hat{p}_z}{\gamma_0}, \quad (22)$$

$$\frac{\mathrm{d}\hat{p}_x}{\mathrm{d}t} = -\frac{\partial \hat{H}}{\partial x} = 0, \quad (23)$$

$$\frac{\mathrm{d}\hat{p}_z}{\mathrm{d}t} = -\frac{\partial \hat{H}}{\partial z} =$$

$$\frac{-k_y \hat{A}_{wy}\sin{(k_y z)}(\hat{p}_x - \hat{A}_{wy}\cos{(k_y z)})}{\gamma_0}$$

$$+\frac{k_x \hat{A}_{wx}\sin{(k_x z)}(\hat{p}_y + \hat{A}_{wx}\cos{(k_x z)})}{\gamma_0}. \quad (24)$$

The fixed points, or steady-state orbits, denoted by $\hat{p}_{z0}$ and z_0, satisfy the steady-state equations of motion and so the following calculation can be made

$$\frac{\mathrm{d}x}{\mathrm{d}t} = \frac{(\hat{p}_{x0} - \hat{A}_{wy}\cos{(k_y z_0)})}{\gamma} = 0$$

$$\Longrightarrow (\hat{p}_{x0} - \hat{A}_{wy}\cos{(k_y z_0)}) = 0$$

$$\Longrightarrow \hat{p}_{x0} = \hat{A}_{wy}\cos{(k_y z_0)} \quad (25)$$

(the obtained fixed point can be simply inverted to $z_0 = \frac{1}{k_y}\cos^{-1}\left(\frac{\hat{p}_{x0}}{\hat{A}_{wy}}\right) = \frac{1}{k_y}\cos^{-1}\left(\frac{C_2}{\hat{A}_{wy}}\right)$) and

$$\frac{\mathrm{d}z}{\mathrm{d}t} = 0 = \frac{\hat{p}_{z0}}{\gamma} \implies \hat{p}_{z0} = 0, \quad (26)$$

$$\frac{\mathrm{d}\hat{p}_z}{\mathrm{d}t} = -k_y \hat{A}_{wy}\sin{(k_y z_0)}(\hat{p}_{x0} - \hat{A}_{wy}\cos{(k_y z_0)})$$

$$+k_x \hat{A}_{wx}\sin{(k_x z_0)}(\hat{p}_{y0} + \hat{A}_{wx}\cos{(k_x z_0)}) = 0. \quad (27)$$

One can write (27) simply as

$$-k_y \hat{A}_{wy}\sin{(k_y z_0)}(C_2 - \hat{A}_{wy}\cos{(k_y z_0)})$$

$$+k_x \hat{A}_{wx}\sin{(k_x z_0)}(C_3 + \hat{A}_{wx}\cos{(k_x z_0)}) = 0. \quad (28)$$

It worth mentioning that one can solve equations (22) and (23) analytically. Substituting (22), i.e., $\mathrm{d}z/\mathrm{d}t = \hat{p}_z/\gamma_0$, into (23) gives

$$\frac{\mathrm{d}\hat{p}_z}{\mathrm{d}t} = \frac{\mathrm{d}\hat{p}_z}{\mathrm{d}z}\frac{\mathrm{d}z}{\mathrm{d}t} = \frac{\hat{p}_z}{\gamma_0}\frac{\mathrm{d}\hat{p}_z}{\mathrm{d}z} =$$

$$\frac{-k_y \hat{A}_{wy}\sin{(k_y z)}(\hat{p}_x - \hat{p}_z)}{\gamma_0}$$

$$+\frac{k_x \hat{A}_{wx}\sin{(k_x z)}(\hat{p}_y + \hat{A}_{wx}\cos{(k_x z)})}{\gamma_0}, \quad (29)$$

therefore

$$\hat{p}_z \, \mathrm{d}\hat{p}_z = \Big[-k_y \hat{A}_{wy}\sin{(k_y z)}(\hat{p}_x - \hat{A}_{wy}\cos{(k_y z)})$$

$$+k_x \hat{A}_{wx}\sin{(k_x z)}(\hat{p}_y + \hat{A}_{wx}\cos{(k_x z)})\Big] \mathrm{d}z. \quad (30)$$

Integrating both sides $\int \mathrm{d}\hat{p}_z \ \hat{p}_z = \int \mathrm{d}z \ (\dots)$, one yields

$$\frac{\hat{p}_z^2}{2} = \hat{A}_{wy}\hat{p}_x\cos{(k_y z)} - \hat{A}_{wx}\hat{p}_y\cos{(k_x z)}$$

$$+\frac{\hat{A}_{wy}^2 k_y}{2}\sin^2{(k_y z)} + \frac{\hat{A}_{wx}^2 k_x}{2}\sin^2{(k_x z)} + \text{const}, \quad (31)$$

so

$$\hat{p}_z = \pm\Big[2\hat{A}_{wy}\hat{p}_x\cos{(k_y z)} - 2\hat{A}_{wx}\hat{p}_y\cos{(k_x z)}$$

$$+\hat{A}_{wy}^2 k_y\sin^2{(k_y z)} + \hat{A}_{wx}^2 k_x\sin^2{(k_x z)} + \text{const}\Big]^{\frac{1}{2}}. \quad (32)$$

3. Numerical simulation

The set of equations of motion derived in the previous section is solved numerically in the following procedure. First, we consider an autonomous system defined by N simultaneous differential equations

$$\frac{\mathrm{d}y_1}{\mathrm{d}t} = f_1(y_1, \dots, y_n),$$

$$\vdots$$

$$\frac{\mathrm{d}y_n}{\mathrm{d}t} = f_n(y_1, \dots, y_n). \quad (33)$$

A solution can be represented by a curve or a trajectory in an N-dimensional phase space. The successive intersections of the trajectory with the surface Σ defined by $y_n - u = 0$, where u is a constant, are considered. It is not possible to specify in advance the variation of the dependent variable y_n over one integration step. This method is able to overcome
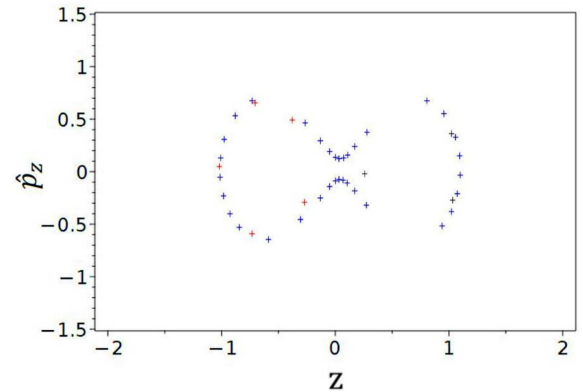

Fig. 2. Poincaré surface-of-section plots in the z–$\hat{p}_z$ plane at $\hat{p}_r = 0$, for $\hat{H} = 6.0$, $\hat{A}_{wx} = \hat{A}_{wy} = 1.0$, $\lambda_x = 2\lambda_y = 6.0$, and $\Omega = 0.0$.
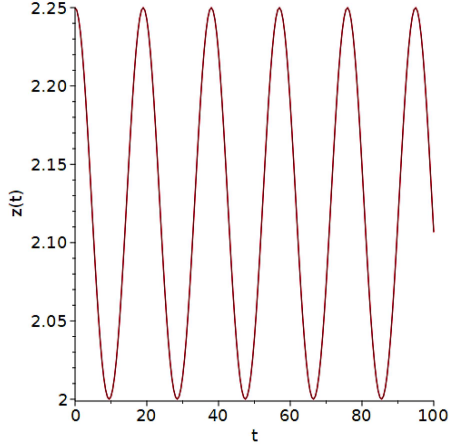
Fig. 3. The behavior of the position z as a function of time, i.e., $z(t)$, where $\hat{A}_{wx} = \hat{A}_{wy} = 1.0$, $\lambda_x = 2\lambda_y = 6.0$, and $\Omega = 0.0$.
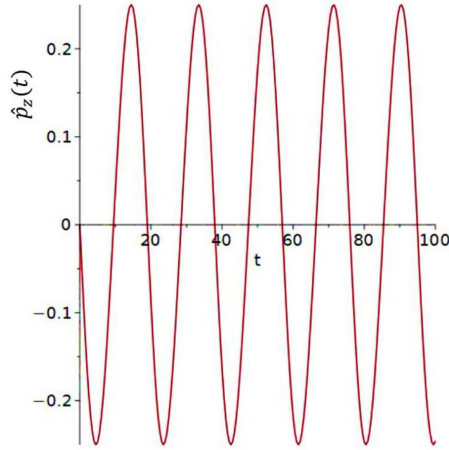

Fig. 4. The behavior of the momentum $\hat{p}_z$ as a function of time, i.e., $\hat{p}_z(t)$, where $\hat{A}_{wx} = \hat{A}_{wy} = 1.0$, $\lambda_x = 2\lambda_y = 6.0$, and $\Omega = 0.0$.

Fig. 5. 3D plot of the surface of section of $\hat{p}_z$ vs z and t.

Fig. 6. 3D plot of the surface of section of $\hat{p}_z$ vs z and t with three fixed values of the Hamiltonian (the black, the blue, and the red).

the problem by dividing the $(n-1)$ equations by the last one, resulting in a new set of equations in which t is considered a dependent variable. The system of equations is integrated until a change in sign is detected for $y_n - u = S$, then one shifts to the new system for one step, taking $\Delta y_n = -S$ as an integration step. This is what is called Hénon's trick. This trick brings us exactly to the surface of section.

Figure 2 shows the Poincaré surface-of-section plots in the z–$\hat{p}_z$ plane at $\hat{p}_r = 0$ for $\hat{H} = 6.0$, $\hat{A}_{wx} = \hat{A}_{wy} = 1.0$, $\lambda_x = 2\lambda_y = 6.0$, and $\Omega = 0.0$ (no axial field) with different initial conditions. It is evident that these contours represent regular trajectories.

Figures 3 and 4 show the smooth behavior of both $z(t)$ and $\hat{p}_z(t)$ as functions of time, so the motion and the orbits are uniform as the axial magnetic field is still zero ($\hat{A}_{wx} = \hat{A}_{wy} = 1.0$, $\lambda_x = 2\lambda_y = 6.0$ and $\Omega = 0.0$).
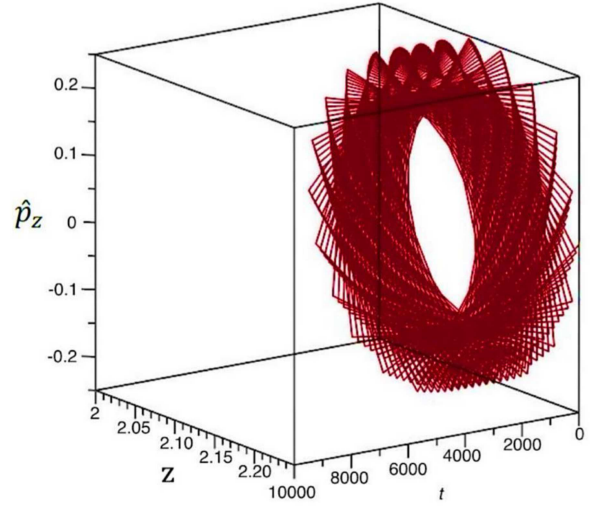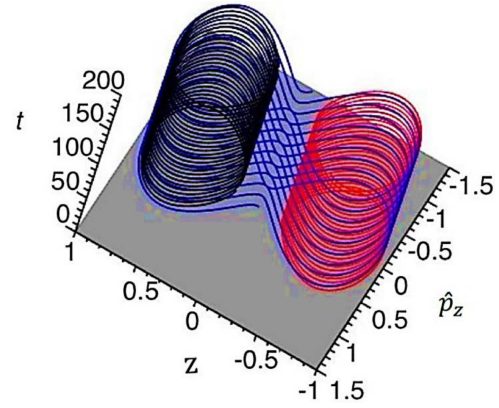
In Fig. 5, a 3D plot of the surface of section of $\hat{p}_z$ vs z and t is shown. It is evident that these contours represent regular trajectories.

Another result regarding the change in the momentum and space with time is shown in Fig. 6 with three values of the Hamiltonian (the black, the blue, and the red); again, the contours represent regular trajectories. The axial field is zero.

The effect of the strength of the axial guide magnetic field is examined by plotting the Poincaré surface-of-section maps generated by numerically integrating the equations of motion expressed by (8)–(12). This analysis demonstrated the chaotic motion and regular motion under certain values of the axial field. Figures 7 and 8 show chaotic electron trajectories for $\Omega = 2.0$ and $\Omega = 4.0$, where it is clear that the axial field exhibits irregular orbit motion. Meanwhile, the large value of the axial field results in nonchaotic motion, as shown in Fig. 9 ($\Omega = 60.0$).
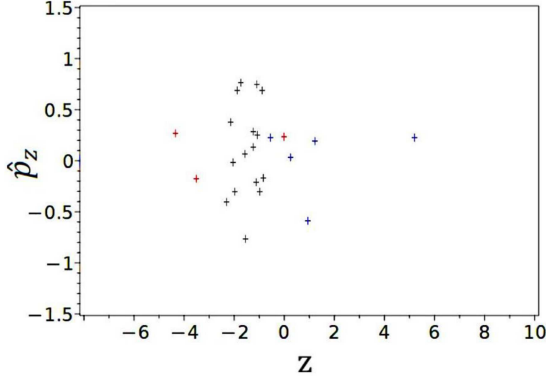
Fig. 7. Poincaré surface-of-section plots in the z–$\hat{p}_z$ plane at $\hat{p}_r = 0$, for $\hat{H} = 6.0$, $\hat{A}_{wx} = \hat{A}_{wy} = 1.0$, $\lambda_x = 2\lambda_y = 6.0$, and $\Omega = 2.0$.
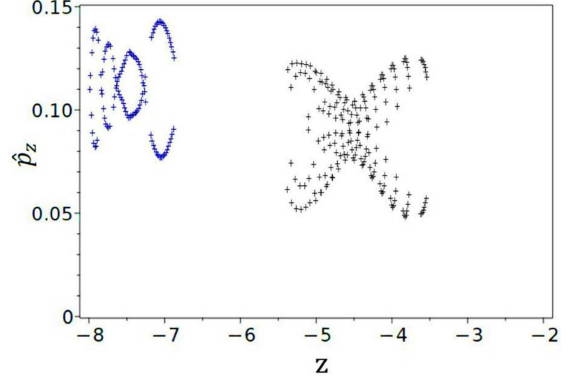

Fig. 9. Poincaré surface-of-section plots in the z–$\hat{p}_z$ plane at $\hat{p}_r = 0$, for $\hat{H} = 6.0$, $\hat{A}_{wx} = \hat{A}_{wy} = 1.0$, $\lambda_x = 2\lambda_y = 6.0$, and $\Omega = 60.0$.

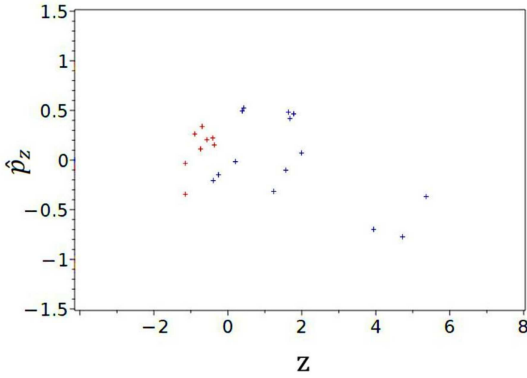Figures 7 and 8 show chaotic electron trajectories for $\Omega = 2.0$ and $\Omega = 4.0$, where it is clear that the axial field exhibits irregular orbit motion. Meanwhile, the large value of the axial field results in non-chaotic motion, as shown in Fig. 9 ($\Omega = 60.0$). The presented results show that dual-undulator systems provide strong chaotic orbits under certain values of the guiding field. As a result, the system of the dual-wiggler free-electron laser without an axial guide magnetic field is integrable, and the contours represent regular trajectories (regular orbits are observed clearly for large values of the axial field), while the system becomes chaotic and the motion is irregular for certain values of the guiding field. The extension of the free-electron laser's wavelength range is an important issue in the FEL research field at present. Utilizing the higher harmonics is one of the ways to obtain a short wavelength, however, it should be operating under certain conditions to avoid harmful chaotic effects. We have demonstrated theoretically that a dual-undulator FEL has one more advantage than a plane-polarized undulator FEL, as it produces regular orbits once the axial field is excluded. For future work, it would be useful if the effect of self-fields was examined.

Fig. 8. Poincaré surface-of-section plots in the z–$\hat{p}_z$ plane at $\hat{p}_r = 0$, for $\hat{H} = 6.0$, $\hat{A}_{wx} = \hat{A}_{wy} = 1.0$, $\lambda_x = 2\lambda_y = 6.0$, and $\Omega = 4.0$.

4. Conclusions

Poincaré surface-of-section maps have been generated by numerically integrating the equations of motion expressed in (8)–(12). This analysis demonstrated the chaotic motion. As we have already noted, the dual-wiggler field induces chaos once the axial guide field is included. The motion described by (8)–(12) occurs in three-dimensional phase space $(z\hat{p}_x\hat{p}_z)$. Figure 2 shows the Poincaré surface-of-section plots in the z–$\hat{p}_z$ plane at $\hat{p}_r = 0$, for $\hat{H} = 6.0$, $\hat{A}_{wx} = \hat{A}_{wy} = 1.0$, $\lambda_x = 2\lambda_y = 6.0$, and $\Omega = 0.0$ (no axial field) with different initial conditions. It is evident that these contours represent regular trajectories with different initial conditions, while the effects of the self-field are neglected and the axial guide magnetic field is not included. To examine the effect of the axial guide magnetic field on the system, we plotted the Poincaré surface-of-section maps generated by numerically integrating the equations of motion expressed by (8)–(12). This analysis demonstrated the chaotic motion and regular motion under certain values of the axial field.

References

[1] H.P. Freund, R.K. Parker, in: *Encyclopedia of Physical Science and Technology*, 3rd ed., Ed. R.A. Meyers, Academic Press, 2003 p. 377.

[2] M. Esmaeilzadeh, J.E. Willett, *Phys. Plasmas* **14**, 033102 (2007).

[3] T. Mohsenpour, H.E. Amri, Z. Norouzi, *Int. J. Opt. Photon.* **10**, 91 (2016).

[4] T.C. Marshall, *Free-Electron Laser*, Macmillan, New York 1985, p. 2.

[5] P. Uddholm, J.E. Willett, S. Bilikmen, *J. Phys. D* **24**, 1278 (1991).

[6] O.Y. Gorobtsov, G. Mercurio, F. Capo-tondi et al., *Nat. Commun.* **9**, 4498 (2018).

[7] L. Peng, Z. Yang S. Liu, *Opt. Commun.* **98**, 285 (1993).

[8] W.B. Colson, *IEEE J. Quant. Electron.* **17**, 1417 (1981).

[9] W.J. Schmitt, C.J. Elliott, *Phys. Rev. A* **41**, 3853 (1990).

[10] B. Girard, Y. Lapierre, J.M. Ortega, C. Bazin, M. Billardon, P. Elleaume, M. Bergher, M. Velghe, Y. Petroff, *Phys. Rev. Lett.* **53**, 2405 (1984).

[11] A.A. Varfolomeev, M.M. Pitatelev, *Nucl. Inst. Methods A* **304**, 507 (1991).

[12] S. Bilikmen, M. Abu Safa, *Phys. Scr.* **50**, 125 (1994).

[13] Y.-P. Ji, S.-J. Wang, J.-Y. Xu, Y.-G. Xu, X.-X. Liu, H. Lu, X.-L. Huang, S.-C. Zhang, *Chinese Phys. B* **23**, 024103 (2014).

[14] R.Z. Sagdeev, D.A. Usikov, G.M. Za-slavsky, *Nonlinear Physics from Pendulum to Turbulence and Chaos*, Harwood Academic Publishers, 2nd printing, 1990, p. 125.

[15] S.-K. Nam, K.-B. Kim, *J. Korean Phys. Soc.* **58**, 22 (2011).

[16] M. Abu Safa, *Int. J. Phys. Sci.* **9**, 459 (2014).

[17] M.V. Berry, *AIP Conf. Proc.* **46**, 16 (1978).

[18] A.J. Lichtenberg, M.A. Lieberman, *Regular and Stochastic Motion*, SpringerVerlag, New York 1983.

[19] H. Goldstein, *Classical Mechanics*, Addison-Weslely, 1980.

[20] A. Taghavi, M. Esmaeilzadeh, *Canadian J. Physics.* **101**, 17 (2022).

[21] S.M. Cavaletto, D. Keefer, S. Mukamel, *Phys. Rev. X* **11**, 011029 (2021).